Region-Enhanced Imaging for Sparse-Aperture Passive Radar

Müjdat Çetin[a] and Aaron D. Lanterman[b]

[a]Laboratory for Information and Decision Systems, Massachusetts Institute of Technology, 77 Massachusetts Ave., Cambridge, MA 02139, USA

[b]School of Electrical and Computer Engineering, Georgia Institute of Technology, Mail Code 0250, Atlanta, GA 30332, USA

ABSTRACT

We present the application of a recently-developed region-enhanced synthetic aperture radar (SAR) image reconstruction technique to the problem of passive radar imaging. One goal in passive radar imaging is to form images of aircraft using signals transmitted by commercial radio and television stations, which then get reflected from the objects of interest. This involves reconstructing an image from sparse samples of its Fourier transform. Due to the sparse nature of the aperture, a conventional image formation approach based on direct Fourier transformation results in quite dramatic artifacts in the image, as compared to the case of active SAR imaging. The region-enhanced image formation method we consider appears to significantly reduce such artifacts, and preserve the features of the imaged object. Furthermore, this approach exhibits robustness to measurement noise. We demonstrate our results using data based on electromagnetic simulations.

Keywords: Passive radar, multistatic radar, sparse-aperture imaging, image reconstruction, feature-enhanced imaging.

1. INTRODUCTION

Traditional synthetic aperture radar (SAR) systems transmit waveforms and deduce information about targets by measuring and analyzing the reflected signals. The active nature of such radars can be problematic in military scenarios since the transmission reveals both the existence and the location of the transmitter. An alternative approach is to exploit "illuminators of opportunity" such as commercial television and AM/FM radio broadcasts. Such passive approaches offer numerous advantages. The overall system cost may be cheaper, since a transmitter is no longer needed. Commercial transmitters are typically much higher in elevation than the prevailing terrain, yielding coverage of low altitude targets. Most importantly, such a system may remain covert, yielding increased survivability and robustness against deliberate directional interference. Such passive multistatic radar systems have been developed to detect and track aircraft. If one could additionally form images from such data, that would be useful in identifying the observed aircraft through image-based target recognition.

We should note that television and FM radio broadcasts operate at wavelengths that are much larger than those typically employed in active radar systems. For instance, an X-band radar might operate at 10 GHz, whereas a passive radar system operates in the VHF and UHF bands (55-885 MHz). From an imaging viewpoint, lower frequencies result in reduced cross-range resolution; hence, to achieve high-resolution images, the target needs to be tracked for some length of time to obtain data over a wide range of angles. Another consequence is that low-frequency images contain extended features, and are not well-modeled by a small number of scattering centers.

Forming images of aircraft using passive radar systems involves reconstructing an image from sparse samples of its Fourier transform.[1,2] The sampling pattern in a particular data collection scenario depends on the locations of the transmitters and the receiver, as well as the flight path of the object to be imaged; hence it is highly variable. Conventional Fourier transform-based imaging essentially sets the unavailable (due to the sparse aperture) data

Further author information: (Send correspondence to Müjdat Çetin.)
Müjdat Çetin: E-mail: mcetin@mit.edu
Aaron D. Lanterman: E-mail: lanterma@ece.gatech.edu

samples to zeros. This results in various artifacts in the formed image, the severity of which depends on the specifics of the data collection scenario.

Motivated by the limitations of direct Fourier transform-based imaging in the context of passive radar, an alternative idea of using a deconvolution technique borrowed from radio astronomy (namely the CLEAN algorithm[3, 4]) has been explored in Ref. 1. However, the results of the study in Ref. 1 suggest that the CLEAN algorithm does not outperform direct Fourier reconstruction for passive radar imaging, due to the following reasons. Deconvolution techniques such as the CLEAN algorithm, work best on images which are well-modeled as a set of distinct point scatterers. Hence, such algorithms are well-suited to high-frequency imaging of man-made targets, as the current on the scatterer surface tends to collect at particular points. When using low frequencies of interest in passive radar, the images are more spatially-distributed. In addition, the complex-valued, and potentially random-phase[5] nature of radar imaging also presents a complication for CLEAN.

To address these challenges, we adapt and use a recently-developed, optimization-based radar imaging method. This approach uses an explicit model of the particular data collection scenario. This model-based aspect provides significant reduction in the types of artifacts observed in conventional imaging. More importantly, the optimization framework contains non-quadratic constraints for region-based feature enhancement, which in turn results in accurate reconstruction of spatially-extended features. Finally, this approach explicitly deals with the complex-valued and potentially random-phase nature of radar signals. We present experimental results on data obtained through electromagnetic simulations via the Fast Illinois Solver Code (FISC), demonstrating the effectiveness of the proposed approach for passive radar imaging.

2. DATA COLLECTION IN PASSIVE RADAR

In multistatic passive radar, the transmitters and the receiver are separated. The "look angle" is then determined by the bisector of the angle formed by the receiver-target-transmitter triangle.[6] The location and support of the data observed in the spatial frequency domain depends on the frequency and bandwidth of the transmitted signals, as well as the look angles. Unlike the case in active radar systems where one uses high-bandwidth signals, in passive radar based on radio and television signals, one is limited to much lower bandwidths. At each observation instant, we might think of each transmitter-receiver pair providing essentially "one point" in the 2-D frequency spectrum. Multiple television and radio stations must be exploited to obtain the frequency diversity needed for reasonable-quality imaging. In addition, the aircraft must be tracked and data collected over time to obtain angular diversity, with each transmitter-receiver pair providing data on an arc in 2-D Fourier space.

In active synthetic aperture radar, one conventional image formation technique is the polar format algorithm based on an interpolation of the data to a rectangular grid, followed by a Fourier transformation. We can consider a similar approach as the "conventional" method for imaging in passive radar. In active monostatic radar imaging, the data in the spatial frequency domain usually lie in a regular annular region. The regularity of this region then leads to a sinc-like point spread function when the image is formed using a Fourier transform. On the other hand, in multistatic passive radar, the "sampling pattern" in the spatial frequency domain is much more irregular for a number of reasons. First of all, since the transmitted signals are narrowband, each transmitter-receiver pair provides a "point" rather than a "slice" of data. Secondly, to obtain reasonable azimuth resolution, data are collected over a wider range of observation angles. Thirdly, the look angles of different transmitter-receiver pairs lead to coverage in different areas of the spectrum. In a related fashion, where the data lie in the spectrum depends on the flight path of the object being imaged. As a result, when we form images using direct Fourier inversion, the imaging artifacts that we encounter are more severe than the case in active radar systems. Furthermore, the nature of the artifacts cannot be determined just based on the system design, since the flight path of the aircraft has a role as well.

3. REGION-ENHANCED IMAGING

Based on the issues outlined in the previous section, we propose a different approach for passive radar imaging. There are two main ingredients of this approach that make it especially suited for passive radar applications. First, it is model-based, meaning that it explicitly uses a mathematical model of the particular observation process. As a result, it has a chance of preventing the types of artifacts that are caused by direct Fourier

inversion. Second, it facilitates the incorporation of prior information or constraints about the nature of the scenes being imaged. This is important, since passive radar imaging is inherently an ill-posed problem. In particular, we focus on the prior information that in the low frequencies of interest in passive radar, the scenes contain spatially-extended structures, corresponding to the actual contours of real aircraft. As a result, we incorporate constraint for preserving and enhancing *region-based* features, such as object contours.

The approach we use for passive radar imaging is based on the feature-enhanced image formation framework of Ref. 7, which is built upon non-quadratic optimization. This approach has previously been used in active synthetic aperture radar imaging. In this section, we provide a brief overview of feature-enhanced imaging. Let us start from the following assumed discrete model for the observation process:

$$\mathbf{g} = \mathbf{T}\mathbf{f} + \mathbf{w} \tag{1}$$

where $\mathbf{g}$ denotes the observed passive radar data, $\mathbf{f}$ is the unknown sampled reflectivity image, $\mathbf{w}$ is additive measurement noise, all column-stacked as vectors, and $\mathbf{T}$ is a complex-valued observation matrix. The data can be in the spatial frequency domain, in which case $\mathbf{T}$ would be an appropriate Fourier transform-type operator corresponding to the particular sampling pattern determined by the flight path of the target. Alternatively through a Fourier transform, one can bring the data into the spatial domain, and then use the resulting transformed observations as the input to the algorithm. In this case $\mathbf{T}$ would be the point spread function corresponding to the particular data collection scenario. In our experiments we use the latter setup.

The objective of image reconstruction is to obtain an estimate of $\mathbf{f}$ based on the data $\mathbf{g}$ in Eqn. (1). The conventional image formation algorithm can roughly be interpreted in this framework as the application of the adjoint to the data: $\hat{\mathbf{f}}_{\mathrm{CONV}} = \mathbf{T}^H\mathbf{g}$. In contrast, feature-enhanced image reconstruction is achieved by solving an optimization problem of the following form:

$$\hat{\mathbf{f}} = \arg\min_{\mathbf{f}} \left\{ \|\mathbf{g} - \mathbf{T}\mathbf{f}\|_2^2 + \lambda_1 \|\mathbf{f}\|_p^p + \lambda_2 \|\nabla|\mathbf{f}|\|_p^p \right\} \tag{2}$$

where $\|\cdot\|_p$ denotes the ℓ_p-norm ($p \leq 1$), ∇ is a 2-D derivative operator, $|\mathbf{f}|$ denotes the vector of magnitudes of the complex-valued vector $\mathbf{f}$, and λ_1, λ_2 are scalar parameters. The first term in the objective function of Eqn. (2) is a data fidelity term. The second and third terms incorporate prior information regarding both the behavior of the field $\mathbf{f}$, and the nature of the features of interest in the resulting reconstructions. The optimization problem in Eqn. (2) can be solved by using an efficient iterative algorithm,[7] based on half-quadratic regularization.[8]

Each of the last two terms in Eqn. (2) is aimed at enhancing a particular type of feature that is of importance for radar images. In particular, the term $\|\mathbf{f}\|_p^p$ is an energy-type constraint on the solution, and aims to suppress artifacts and increase the resolvability of *point* scatterers. The $\|\nabla|\mathbf{f}|\|_p^p$ term on the other hand, aims to reduce variability in homogeneous *regions*, while preserving and enhancing region boundaries. The relative magnitudes of λ_1 and λ_2 determine the emphasis on such *point-based* versus *region-based* features. Therefore, this framework lets us reconstruct images with two different flavors: using a relatively large λ_1 yields *point-enhanced* imagery, and using a relatively large λ_2 yields *region-enhanced* imagery. In the context of passive radar imaging, our primary focus is to preserve and enhance the shapes of spatially-distributed objects. Hence we emphasize the use of the region-enhancement terms here.

4. EXPERIMENTS

4.1. Electromagnetic Simulation using FISC

Asymptotic codes such as XPATCH[9] do not work well for aircraft-sized targets at the low frequencies of interest in passive radar systems. Hence, the simulations in the remaining sections invoke the Fast Illinois Solver Code (FISC), which solves Maxwell's equations via the method of moments. FISC is extremely particular about the quality of CAD models it needs. In particular, FISC requires that each edge of each triangular facet exactly match the edge of some other triangular facet. The model must contain no internal or intersecting parts. Unfortunately, such models are rare; in particular, readily available models which are perfectly adequate for XPATCH are often not suitable for FISC.

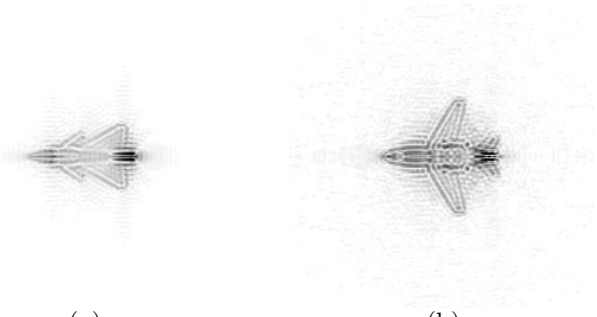

(a) (b)

Figure 1. Reference passive radar images reconstructed from "full" datasets using direct Fourier reconstruction. The images are 256×256. (a) VFY-218. (b) Falcon 20.

Each experiment in this paper is conducted on two different targets: a VFY-218, and a Dassault Falcon 20. A FISC compatible model of the VFY-218 comes standard as part of the SAIC Champaign XPATCH/FISC distribution. For the Falcon 20, we started from a FISC-compatible model of a Falcon 100. The Falcon 20 is essentially a larger version of the Falcon 100, so we used an approximate Falcon 20 model (as done in Ref. 1) by scaling the Falcon 100 model.

Given such models, we construct Fourier datasets through FISC runs. The support of the data in the spatial frequency domain will in general be limited by the observation geometry and system parameters. However, in order to establish an "upper bound" on the expected imaging performance, let us first observe the images we would obtain if we had a "full" dataset. To this end, let us use the Fourier data corresponding to 211.25 MHz (NTSC television channel 13) and incident and observed angles over the full 360 degree viewing circle. Such data would cover a disk in the spatial frequency domain.[1] The magnitudes of the radar images of the two targets, created by inverse Fourier transforming such data are shown in Fig. 1. Of course, such rich data sets would be unavailable in practice. However for us, these reconstructions will serve as the "reference scenes" with which to compare the results of our experiments in the following sections, based on realistic data collection scenarios.

4.2. Experimental Setup

Fig. 2 shows the locations of the VHF television stations and the FM radio stations in the Washington DC area assumed in our simulations. The center of the coordinate system, where our hypothetical receiver is located, is the Lockheed Martin Mission Systems facility in Gaithersburg, MD. Five hypothetical flight paths are shown. The left column of Fig. 3 shows the Fourier "sampling patterns" resulting from this particular transmitter/receiver geometry and for each of the five flight paths. The sampling pattern indicates the support of the observed data in the spatial frequency domain for a particular flight path. Hence the observed data for each flight path consists of a specific subset of the data used for reconstructing the images of Fig. 1, whose contents are determined by the corresponding sampling pattern. The middle and right columns in Fig. 3 show the magnitude of the corresponding point spread functions (PSFs) given by the inverse Fourier transform of the sampling patterns. The middle column shows magnitude on a linear scale, while the right column shows magnitude on a logarithmic scale in order to elucidate low-level detail in the sidelobes. Note that these sampling patterns, or equivalently PSFs, are used in specifying the observation matrix $\mathbf{T}$ in Eqn. (1). In the next section, we present results based on data associated with each of these flight paths.

4.3. Results

Let us first consider the flight path corresponding to the sampling pattern in the bottom row in Fig. 3. The corresponding "conventional" image of the VFY-218, obtained by direct Fourier transformation of the data, is shown in the top row of Fig. 4(a). Points in the spatial frequency domain where observations are unavailable are set to zero. This is equivalent to convolving the reference image in Fig. 1(a) with the PSF in the bottom row of Fig. 3. As compared to the "reference" image of Figure 1(a), the direct Fourier reconstruction in the

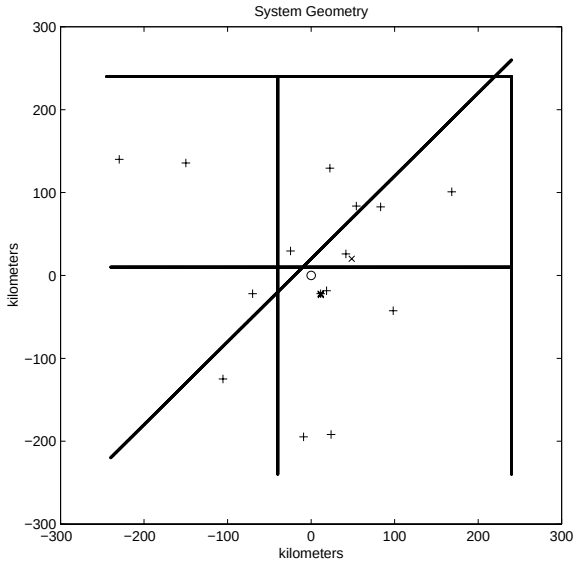

Figure 2. Data collection geometry. VHF TV stations are represented with a +; FM radio stations with a ×, and the receiver with a circle. The lines represent five hypothetical flight paths.

top row of Fig. 4(a) contains severe imaging artifacts, resulting in suppression of some of the characteristic features of the imaged object. In this example we have not added any noise to the measurements. Hence in the context of the observation model in Eqn. (1), we do not have any measurement noise. As a result, one can consider applying the pseudoinverse of the observation matrix, namely $\mathbf{T}^\dagger$, to the data to obtain a reconstruction $\hat{\mathbf{f}}_{\text{PINV}} = \mathbf{T}^\dagger \mathbf{g}$. The pseudoinverse reconstruction obtained in this manner is shown in the top row of Fig. 4(b). The region-enhanced reconstruction (with $p = 1$) is shown in the top row of Fig. 4(c). Both the pseudoinverse and the region-enhanced reconstructions provide reasonable results in this noise-free case, with the region-enhanced reconstruction providing somewhat better suppression of sidelobe artifacts. It is well-known that pseudoinverse solutions are very sensitive to noise, especially when the observation model results in an ill-conditioned matrix. The bottom row of Fig. 4 shows the direct Fourier, the pseudoinverse, and the region-enhanced reconstructions, when we have a small amount of measurement noise. The pseudoinverse solution breaks down in this case, and is in general useless in practical scenarios where observation noise is inevitable. The region-enhanced reconstruction exhibits robustness to noise, and preserves the characteristic features and shape of the VFY-218, despite the noisy sparse-aperture observations.

Let us now consider all the flight paths in Fig. 3. In Fig. 5, we show the reconstructions for the VFY-218. In this example, we have a small amount of measurement noise, resulting in a signal-to-noise ratio (SNR) of 30 dB. Fig. 5(a) and Fig. 5(b) contain the direct Fourier, and the region-enhanced images, respectively. There is a row-to-row correspondence between Fig. 3 and Fig. 5, in terms of the flight paths. We observe that region-enhanced imaging produces reconstructions that preserve the features of the reference image of Fig. 1(a) in a much reliable way than direct Fourier imaging. In all of our experiments, we use $p = 1$ in Eqn. (2) for region-enhanced imaging.

We also observe that the direct Fourier images in the bottom three rows of Fig. 5, while blurry, are clearer than the images in the top two rows. Looking at the corresponding sampling patterns in Fig. 3, the primary difference seems to be that the paths corresponding to the top two rows keep the receiver and the transmitters on the same side of the target, yielding a quasi-monostatic (small bistatic angle) geometry, whereas in the bottom three rows, the target flies between the receiver and some of the transmitters, yielding large bistatic angles and wider effective coverage in frequency space. The important point to note is that the nature of the artifacts that may be caused by direct Fourier imaging depend on the flight path of the target being imaged, hence may not be easily predicted prior to data collection. On the other hand, in Fig. 5 we observe that region-enhanced images corresponding to different flight paths are much more similar. In Fig. 6, we show similar results for the Falcon 20,

again with data having an SNR of 30 dB.

Finally, in Figures 7 and 8, we show reconstructions of the VFY-218 and the Falcon 20 respectively, for a noisier scenario where SNR=10 dB. Region-enhanced imaging appears to produce reasonable results in this case as well.

5. CONCLUSION

We have explored the use of an optimization-based, region-enhanced image formation technique for the sparse-aperture passive radar imaging problem. Due to the sparse and irregular pattern of the observations in the spatial frequency domain, conventional direct Fourier transform-based imaging from passive radar data leads to unsatisfactory results, where artifacts are produced and characteristic features of the imaged objects are suppressed. The region-enhanced imaging approach we use appears to be suited to the passive radar imaging problem for a number of reasons. First, due to its model-based nature, the types of artifacts caused by conventional imaging are avoided. Second, it leads to the preservation and enhancement of spatially-extended object features. Third, unlike a number of deconvolution techniques, it can deal with the complex-valued nature of the signals involved. Our experimental results based on data obtained through electromagnetic simulations demonstrate the effectiveness and promise of this approach for passive radar imaging.

In this paper, we have assumed that we know the passive radar observation model exactly, which involves knowledge about not only the transmitters and the receiver, but also about the flight path of the target being imaged. In practice, information about the target flight path is obtained from a tracking system, and is likely to contain uncertainties. Therefore, it is important to develop image formation techniques that can deal with uncertainties in the observation model. This constitutes a challenging direction for future work.

ACKNOWLEDGMENTS

This work was supported by the Air Force Office of Scientific Research (AFOSR) under Grant F49620-00-0362, and by DARPA under Grant F49620-98-1-0498.

REFERENCES

1. A. D. Lanterman and D. C. Munson, Jr., "Deconvolution techniques for passive radar imaging," in *Algorithms for Synthetic Aperture Radar Imagery IX*, E. G. Zelnio, ed., *Proc. SPIE* **4727**, pp. 166–177, (Orlando, FL, USA), Apr. 2002.
2. Y. Wu and D. C. Munson, Jr., "Multistatic synthetic aperture imaging of aircraft using reflected television signals," in *Algorithms for Synthetic Aperture Radar Imagery VIII*, E. G. Zelnio, ed., *Proc. SPIE* **4382**, (Orlando, FL, USA), Apr. 2001.
3. J. Högbom, "Aperture synthesis with a non-regular distribution of interferometer baselines," *Astronomy and Astrophysics Supplement Series* **15**, pp. 417–426, 1974.
4. U. J. Schwarz, "Mathematical-statistical description of the iterative beam removing technique (method CLEAN)," *Astronomy and Astrophysics* **65**, pp. 345–356, 1978.
5. D. C. Munson Jr. and J. L. C. Sanz, "Image reconstruction from frequency-offset Fourier data," *Proc. IEEE* **72**, pp. 661–669, June 1984.
6. O. Arıkan and D. C. Munson Jr., "A tomographic formulation of bistatic synthetic aperture radar," in *Proceedings of ComCon 88, Advances in Communications and Control Systems*, Oct. 1988.
7. M. Çetin and W. C. Karl, "Feature-enhanced synthetic aperture radar image formation based on nonquadratic regularization," *IEEE Trans. Image Processing* **10**, pp. 623–631, Apr. 2001.
8. D. Geman and G. Reynolds, "Constrained restoration and the recovery of discontinuities," *IEEE Trans. Pattern Anal. Machine Intell.* **14**, pp. 367–383, Mar. 1992.
9. M. Hazlett, D. J. Andersh, S. W. Lee, H. Ling, and C. L. Yu, "XPATCH: a high-frequency electromagnetic scattering prediction code using shooting and bouncing rays," in *Targets and Backgrounds: Characterization and Representation*, W. R. Watkins and D. Clement, eds., *Proc. SPIE* **2469**, pp. 266–275, (Orlando, FL, USA), Apr. 1995.

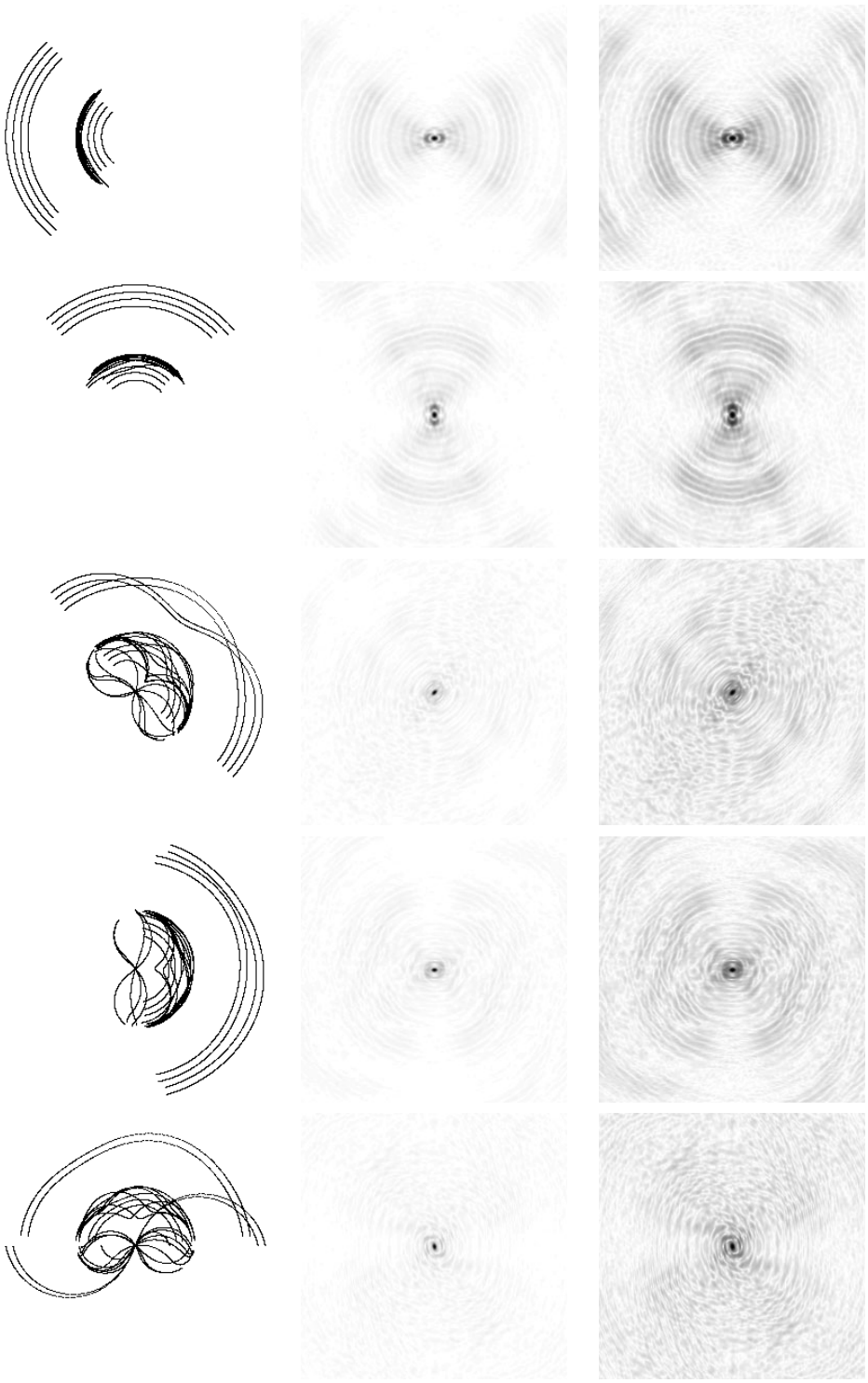

Figure 3. Left column shows Fourier sampling patterns associated with five different flight paths. Remaining columns show the magnitude of the PSFs associated with the sampling patterns. The middle column uses a linear scale, while the right column uses a logarithmic scale to show fine detail. The PSFs are 256×256.

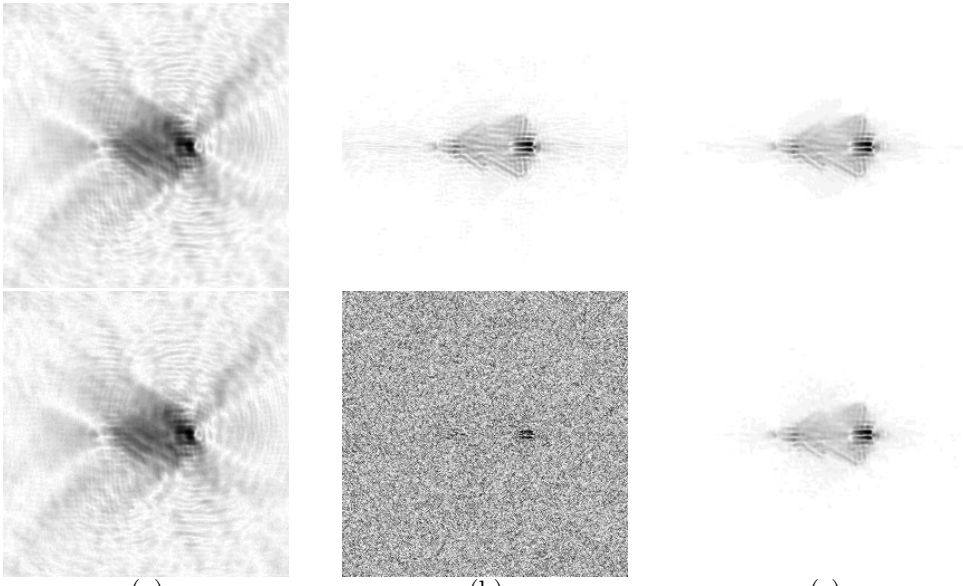

(a) (b) (c)

Figure 4. Reconstructions of the VFY-218 based on data restricted to the Fourier sampling pattern shown in the bottom row of Fig. 3. Top row: noiseless data. Bottom row: noisy data. (a) Direct Fourier reconstruction. (b) Pseudoinverse reconstruction. (c) Region-enhanced reconstruction ($p = 1$).

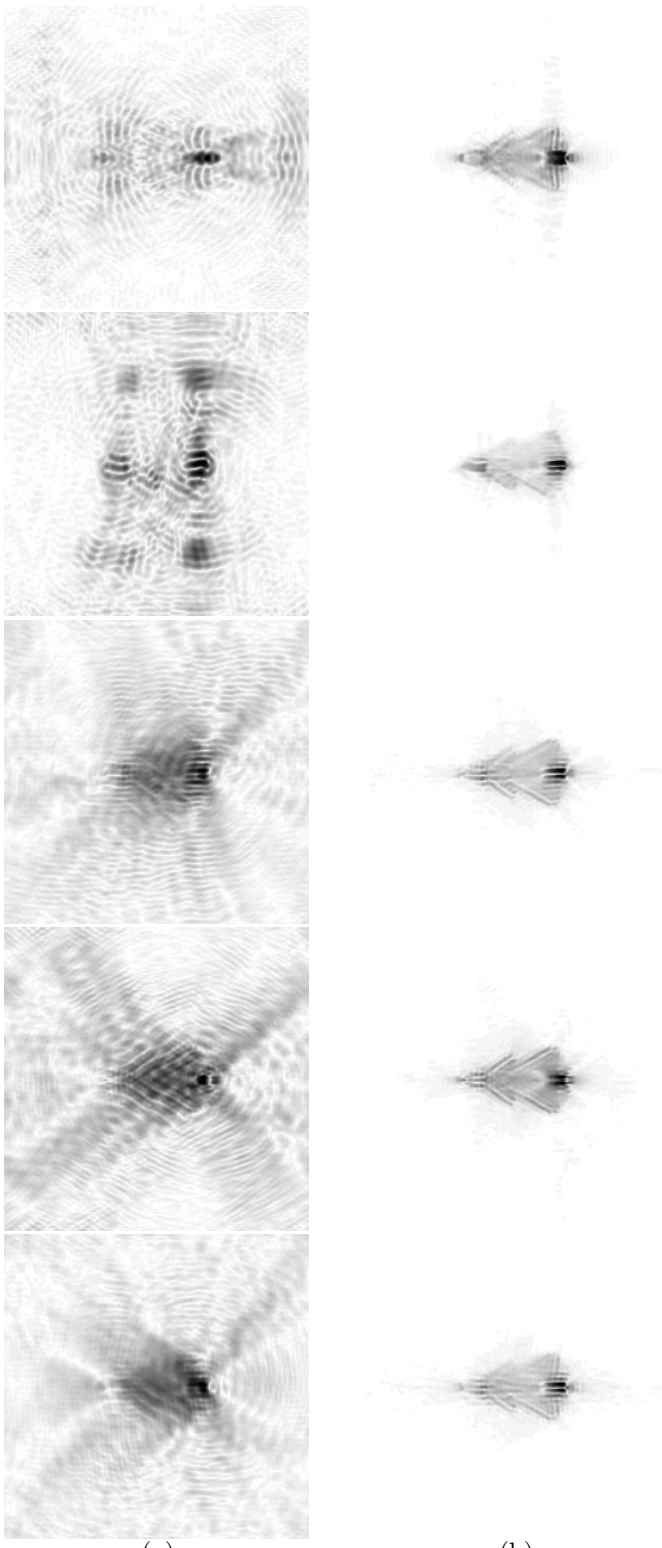

(a) (b)

Figure 5. Reconstructions of the VFY-218 based on data (with SNR = 30 dB) restricted to the Fourier sampling patterns shown in Fig. 3. (a) Direct Fourier reconstructions. (b) Region-enhanced reconstructions ($p = 1$).

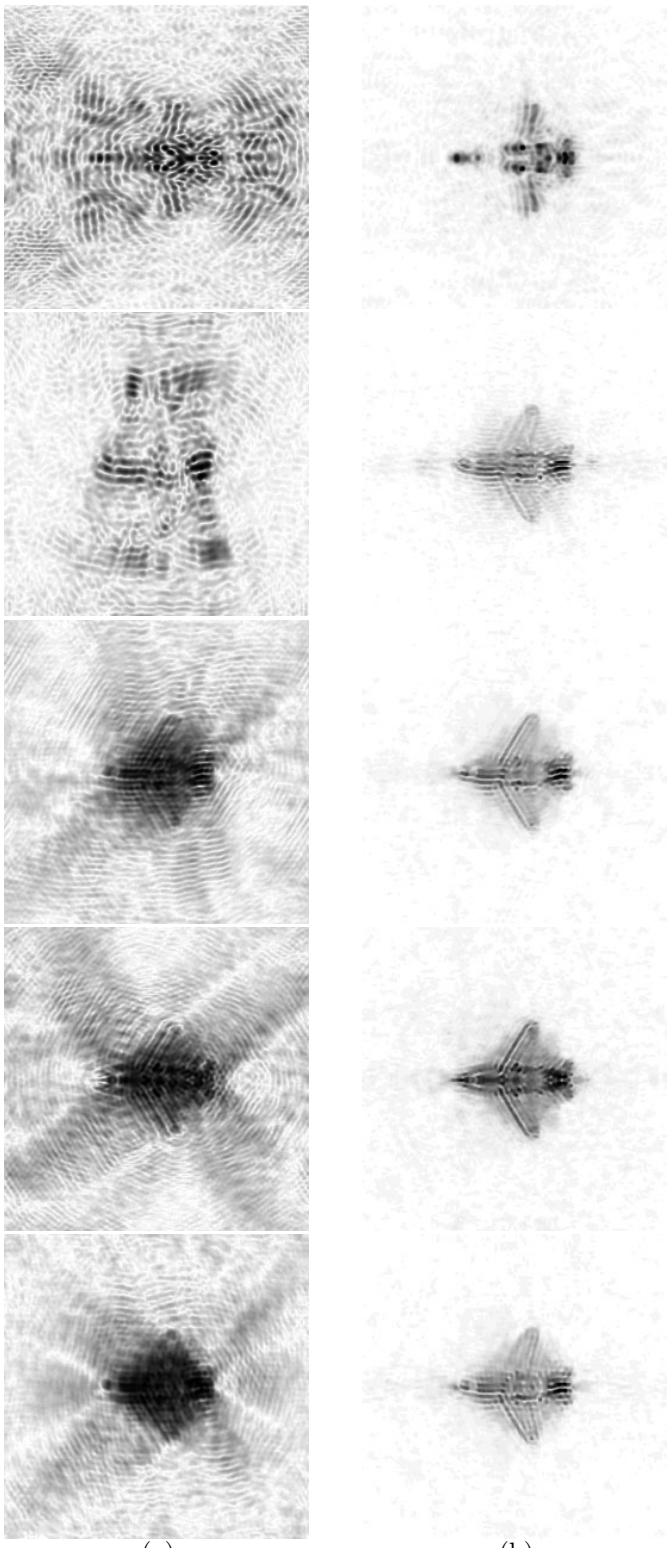

(a) (b)

Figure 6. Reconstructions of the Falcon 20 based on data (with SNR = 30 dB) restricted to the Fourier sampling patterns shown in Fig. 3. (a) Direct Fourier reconstructions. (b) Region-enhanced reconstructions ($p = 1$).

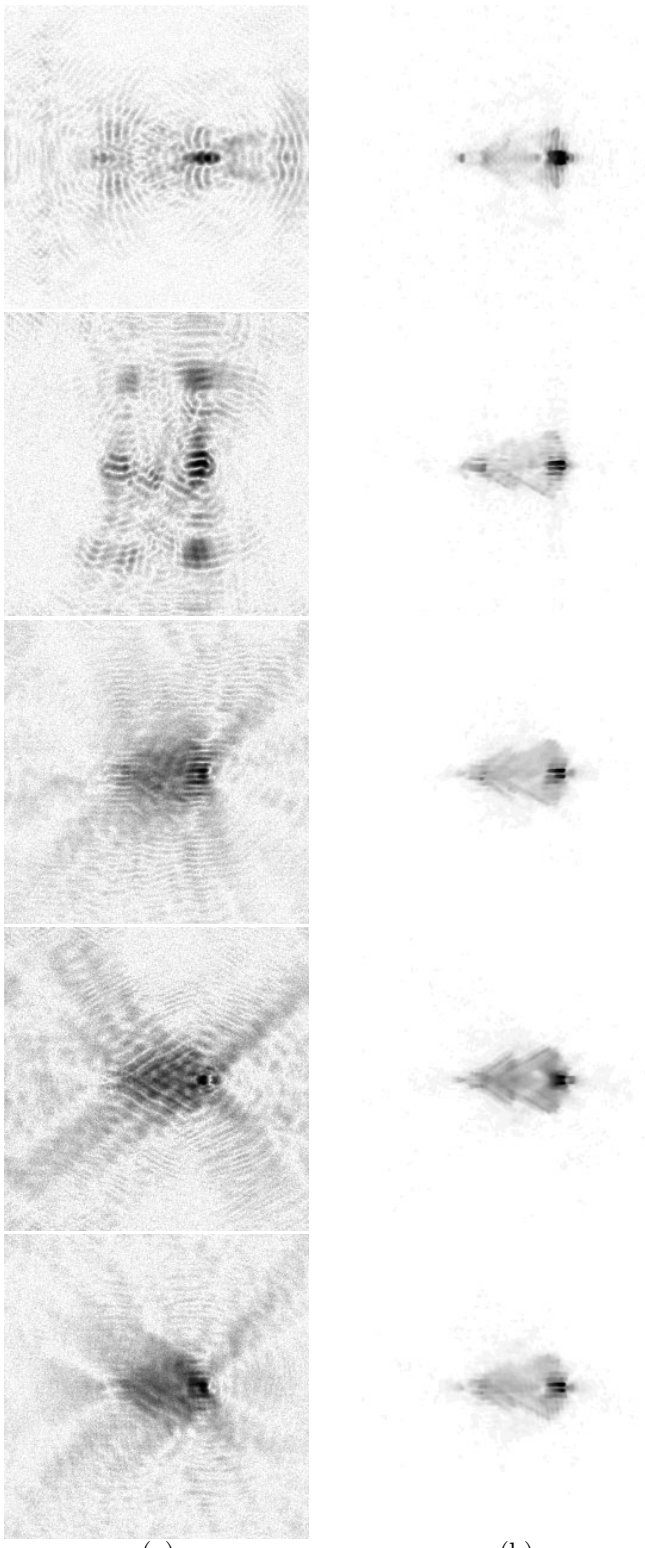

(a) (b)

Figure 7. Reconstructions of the VFY-218 based on data (with SNR = 10 dB) restricted to the Fourier sampling patterns shown in Fig. 3. (a) Direct Fourier reconstructions. (b) Region-enhanced reconstructions ($p = 1$).

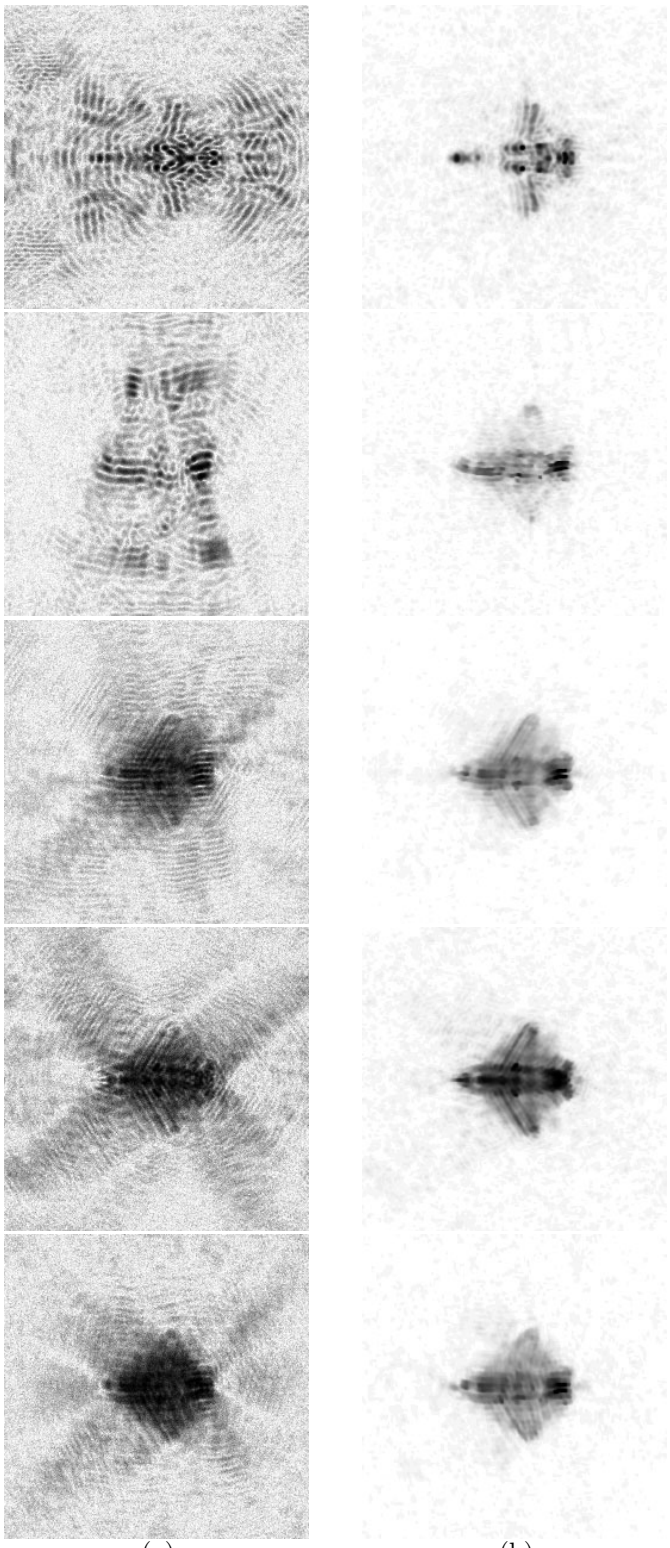

(a) (b)

Figure 8. Reconstructions of the Falcon 20 based on data (with SNR = 10 dB) restricted to the Fourier sampling patterns shown in Fig. 3. (a) Direct Fourier reconstructions. (b) Region-enhanced reconstructions ($p = 1$).